ELSEVIER

NeuroImage

www.elsevier.com/locate/ynimg
NeuroImage 30 (2006) 1149 – 1160

Cortical layer-dependent BOLD and CBV responses measured by spin-echo and gradient-echo fMRI: Insights into hemodynamic regulation

Fuqiang Zhao,[a] Ping Wang,[a] Kristy Hendrich,[a] Kamil Ugurbil,[b] and Seong-Gi Kim[a,*]

[a]*Department of Neurobiology, University of Pittsburgh, Pittsburgh, PA 15203, USA*
[b]*Center for Magnetic Resonance Research, University of Minnesota, Minneapolis, MN 55455, USA*

Received 28 July 2005; revised 6 November 2005; accepted 10 November 2005
Available online 18 January 2006

Spatial specificity of functional magnetic resonance imaging (fMRI) signals to sub-millimeter functional architecture remains controversial. To investigate this issue, high-resolution fMRI in response to visual stimulus was obtained in isoflurane-anesthetized cats at 9.4 T using conventional gradient-echo (GE) and spin-echo (SE) techniques; blood oxygenation-level dependent (BOLD) and cerebral blood volume (CBV)-weighted data were acquired without and with injection of 10 mg Fe/kg monocrystalline iron oxide nanoparticles (MION), respectively. Studies after MION injection at two SE times show that the T_2' contribution to SE fMRI is minimal. GE and SE BOLD changes were spread across the cortical layers. GE and SE CBV-weighted fMRI responses peaked at the middle cortical layer, which has the highest experimentally-determined microvascular volume; full-width at half-maximum was <1.0 mm. Parenchymal sensitivity of GE CBV-weighted fMRI was ~3 times higher than that of SE CBV-weighted fMRI and ~1.5 times higher than that of BOLD fMRI. It is well known that GE CBV-weighted fMRI detects a volume change in vessels of all sizes, while SE CBV-weighted fMRI is heavily weighted toward microvascular changes. Peak CBV change of 10% at the middle of the cortex in GE measurements was 1.8 times higher than that in SE measurements, indicating that CBV changes occur predominantly for vasculature connecting the intracortical vessels and capillaries. Our data supports the notion of laminar-dependent CBV regulation at a sub-millimeter scale.

Keywords: fMRI; Hemodynamic response; BOLD; CBV; Cortical layers; Microvessels

Introduction

Functional magnetic resonance imaging (fMRI) techniques have been a method of choice for visualizing neural activity in humans. To date, most fMRI studies have been performed using conventional blood oxygenation level-dependent (BOLD) methodology (Ogawa et al., 1990) with a spatial resolution of several millimeters. However, it is not clear whether neural activity-induced vascular responses are specific to sub-millimeter functional structures. To obtain high-resolution fMRI, the imaging signals should be relatively specific to parenchyma with reduced sensitivity to large vessels. This can be achieved by various data acquisition approaches, including contrast agent administration (Kennan et al., 1998; Mandeville et al., 1998, 2001; van Bruggen et al., 1998) and/or spin-echo (SE) data acquisition at high magnetic fields (Ogawa et al., 1993; Boxerman et al., 1995; Lee et al., 1999, 2002; Kim and Ogawa, 2002). Injection of monocrystalline iron oxide nanoparticles (MION) as an intravascular contrast agent induces a susceptibility effect in and around the vasculature and MION therefore behaves as a plasma blood volume tracer (Kennan et al., 1998; Mandeville et al., 1998, 2001; van Bruggen et al., 1998). This cerebral blood volume (CBV)-weighted fMRI approach has been used to improve the spatial localization of fMRI signals, where the highest gradient-echo (GE) CBV change was observed at the middle of the rat somatosensory cortex, while the highest GE BOLD signal was observed at the surface of the cortex (Mandeville and Marota, 1999; Lu et al., 2004). In our laboratory, a similar result was seen in the cat visual cortex at 4.7 T (Harel et al., 2002b).

To characterize the susceptibility effects on relaxation of GE and SE tissue signals, a number of analytical biophysical models have been developed (Ogawa et al., 1993; Kennan et al., 1994; Weisskoff et al., 1994; Yablonskiy and Haacke, 1994; Kiselev and Posse, 1999; Jensen and Chandra, 2000), and also Monte Carlo simulations have been performed (Ogawa et al., 1993; Boxerman et al., 1995). It should be noted that the intravascular BOLD signal

* Corresponding author. 3025 East Carson Street, Pittsburgh, PA 15203, USA. Fax: +1 412 383 6799.
E-mail address: kimsg@pitt.edu (S.-G. Kim).
Available online on ScienceDirect (www.sciencedirect.com).

1053-8119/$ - see front matter © 2005 Elsevier Inc. All rights reserved.
doi:10.1016/j.neuroimage.2005.11.013

is ignored in these theoretical models and simulations. At high magnetic fields or with injection of susceptibility contrast agents, the intravascular contribution to fMRI signals is indeed negligible (Mandeville and Marota, 1999; Lee et al., 1999; Duong et al., 2003; Yacoub et al., 2003), but it can be significant at magnetic fields of 1.5 T to 4.7 T (van Zijl et al., 1998; Oja et al., 1999; Fujita, 2001). The aforementioned models and simulations of extravascular signals have shown that a change in R_2 (=1/T_2 in SE) is heavily weighted to the microvasculature and that a change in R_2* (=1/T_2* in GE) is sensitive to vessels of all sizes. Thus, by combining different vessel-sensitive SE and GE measurements, it is possible to investigate the vessel-size dependence of CBV-weighted fMRI, and to pinpoint the characteristics of the vasculature involved in blood volume regulation across the cortex.

In this paper, the spatial specificity of BOLD and CBV-weighted fMRI was examined in the visual cortex of isoflurane-anesthetized cats using GE and SE techniques at 9.4 T before and after injection of MION at a dose of 10 mg Fe/kg, respectively. To view the cortical cross-section with in-plane resolution of 156 × 156 μm^2, a 2-mm-thick imaging slice was selected perpendicular to the cortical surface. Since the middle cortical layer is known to have the highest cytochrome oxidase activity, metabolic rate, and density of synapses (Woolsey et al., 1996), the highest signal changes should occur at the middle of the cortex if the imaging signals are specific to metabolic response and/or neural activity. The changes to R_2 and R_2* (ΔR_2 and ΔR_2*) in tissue induced by MION without stimulation are indicative of baseline microvascular-weighted CBV and total CBV values, respectively; these baseline values were compared with ΔR_2 and ΔR_2* induced by CBV changes during visual stimulation. Additionally, CBV-weighted SE fMRI was performed at two different echo times to determine whether any stimulation-induced changes other than ΔR_2 are detectable. Preliminary accounts of this work have been presented (Zhao et al., 2004b).

Materials and methods

Animal preparation

Eight female adolescent cats (weight: 0.76–1.6 kg, 10–16 weeks old) were studied with approval from the University of Minnesota Institutional Animal Care and Use Committee. Cats were anesthetized with intramuscular injection of a ketamine (10–25 mg/kg) and xylazine (2.5 mg/kg) cocktail. The cat was orally intubated and mechanically ventilated using a pressure-driven Kent ventilator (model: RSP-1002, CT) (~29–30 strokes/min) under isoflurane anesthesia (1–1.3% v/v) in a 7:3 N_2O:O_2 mixture. The femoral vein and artery were catheterized. Pancuronium bromide mixed in 5% dextrose Ringer's solution was delivered at 0.4 mg/kg/hr by infusion pump. The cat was placed in a cradle and restrained in normal postural position by a head holder, consisting of ear bars and bite bar. End-tidal CO_2 (Datex Omeda, Helsinki, Finland) was maintained in the range of 3.0–3.8%. During MRI experiments, arterial blood pressure and end-tidal CO_2 were continuously recorded (MP150, BIOPAC Systems Inc., Goleta, CA). Rectal temperature was maintained at 38.5 ± 0.5°C with a feedback hot water circulator. Blood gas analysis was intermittently performed.

For CBV-weighted studies, a bolus of 10 mg Fe/kg dextran-coated MION contrast agent (obtained from Ralph Weissleder's laboratory at the Massachusetts General Hospital) with an average particle diameter of 26–28 nm, was injected intravenously along with ~1.5 ml/kg 10% dextran–40 solution; this agent has a half-life time >6 h in blood (Zhao et al., 2003). A steady-state condition was reached within a few minutes after injection (data not shown).

Visual stimulation

Binocular full-field visual stimuli were presented from a video projector (NEC, model MT1055; resolution 1040 × 890) onto a rear-projection screen. The screen was positioned 15 cm from the cat's eyes, covering about 37° of the visual field. Visual stimuli consisted of square-wave high-contrast moving gratings (2 cycles/s) with low spatial frequency (0.2 cycles/degree) at a selected orientation. During the pre- and post-stimulus periods, a stationary grating pattern with the same orientation was presented. The cat's pupils were dilated with ophthalmic solutions of atropine (1%), phenylephrine hydrochloride (2.5%) and proparacaine hydrochloride (0.5%). Contact lenses (Danker Laboratories Inc., FL) were fitted to the open eyes to prevent corneal drying. Similar experimental setup and visual stimulation were used previously for fMRI studies in our laboratory (Duong et al., 2000a; Kim et al., 2000; Duong et al., 2001; Harel et al., 2002a; Zhao et al., 2004a, 2005).

General MRI experiments

All MRI measurements were performed on a 9.4 T magnet with a clear bore size of 31 cm, driven by a Unity INOVA console (Varian Inc., Palo Alto, CA) at the University of Minnesota. The actively shielded gradient coil was 11-cm inner diameter with a strength of 30 G/cm and a rise time of 300 μs (Magnex, Abington, UK). A 1.6-cm diameter surface coil positioned on top of the cat head provided radiofrequency (RF) transmission and reception. T_1-weighted anatomical images were obtained to identify brain structures by the four-shot SE echo planar imaging (EPI) technique with an inversion time of 1.4 s, echo time (TE) = 17 ms, and repetition time (TR) for each segment of 4 s. The visual cortex was then positioned in the iso-center of the magnet, and the magnetic field homogeneity was optimized by manual shimming.

From multi-slice GE BOLD 'scout' fMRI and anatomical images, a 2-mm thick oblique coronal slice orthogonal to the surface of the visual cortex (see Fig. 1A) was chosen for all functional studies. The phase-encoding direction for EPI was along the dorsal–ventral dimension, and the field of view was 2 × 2 cm^2. For all high-resolution studies, the four-shot EPI technique with a navigator echo and center-out phase-encoding scheme (Kim et al., 1996) was used with matrix size = 128 × 128 and EPI readout time per shot = 33.7 ms. Low-resolution studies (TE-dependent fMRI only) used the one-shot EPI technique to rapidly acquire data with matrix size = 64 × 64 and EPI readout time = 40.9 ms. In GE EPI measurements, the power level of the sinc-shaped RF pulse was adjusted to maximize signal intensity within the visual cortex. SE EPI data were acquired with a double-echo EPI sequence (Lee et al., 1999), where adiabatic half- and full-passage pulses provided 90° excitation and 180° refocusing, respectively. Two experiments were performed: (1) high-resolution SE and GE fMRI without and with MION (i.e., BOLD and CBV-weighted), and (2) low-resolution SE fMRI with two interleaved echo times after MION injection. A total of 8 cats were studied: three for experiment (1) only, two for consecutive experiments (1) and (2), and another three for experiment (2) only.

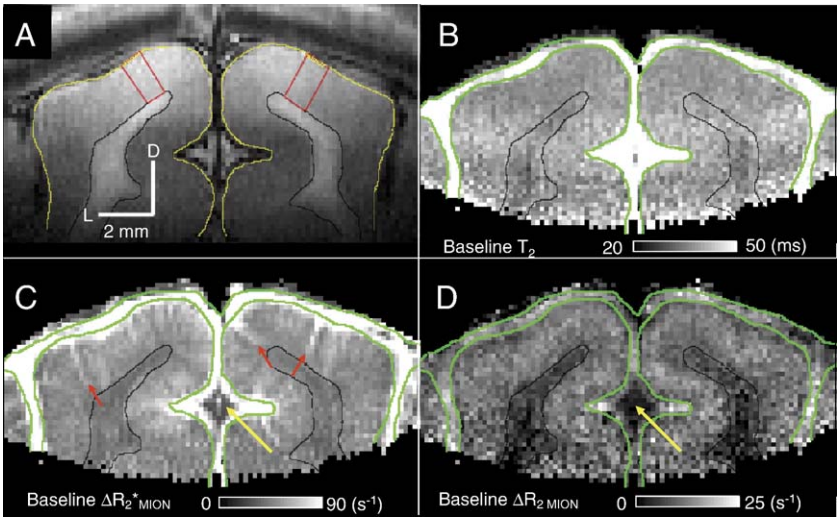

Fig. 1. Basal GE and SE CBV distribution. Illustrative data are from one animal. (A) T_1-weighted anatomical image shows the cortical surface outlined in yellow contours and white matter boundaries are delineated by black contours, then superimposed on remaining images of (Figs. 1, 2, 5 and 6). Two quadrangular regions within visual area 18 were defined (outlined in red) for subsequent cortical depth-dependent analysis. Each region was 700–900 μm wide and ~1.7 mm deep, extending from the surface of the cortex to the white matter. D: dorsal, L: lateral. (B) On the baseline T_2 map (before MION injection), spaces containing CSF appear bright (long T_2 values) and are outlined in green, then superimposed on remaining maps of Figs. 1 and 2. Maps of $\Delta R_2{}^*_{MION}$ and $\Delta R_{2\,MION}$ were obtained from gradient-echo and spin-echo MRI data with injection of 10 mg Fe/kg MION, and indicate distributions of total (C) and microvascular-weighted (D) CBV in the absence of evoked neural activity. While the area with the largest total CBV is located near the surface of the cortex, the region with the highest microvascular-weighted CBV is located within the middle cortical layer. Red arrows (C) indicate intracortical vessels. Yellow arrows (C, D) indicate CSF area where vessels are absent.

Comparison between BOLD and CBV-weighted SE and GE fMRI at high-resolution

Changes in R_2 and R_2* induced by MION without evoked neural activity ($\Delta R_{2\,MION}$ and $\Delta R_2{}^*_{MION}$) can be described by the quantities $k{\cdot}CBV_{SE}$ and $k^*{\cdot}CBV_{GE}$, respectively, where CBV_{SE} and CBV_{GE} represent microvascular-weighted CBV and total CBV, and k and k^* are both constants that are dependent on the concentration of MION in blood (Yablonskiy and Haacke, 1994; Kiselev and Posse, 1999; Tropres et al., 2001). Since MION concentration in blood corresponds to the dose of MION administered, k and k^* are assumed to be spatially homogeneous within the cortex, and therefore maps of $\Delta R_{2\,MION}$ and $\Delta R_2{}^*_{MION}$ directly indicate baseline distributions of microvascular-weighted CBV and total CBV, respectively.

Baseline CBV distributions were obtained with a single injection of MION in five cats. To obtain $\Delta R_{2\,MION}$, SE EPI images were acquired before and after MION injection with TR = 8 s, and TE values of 17, 19, 21, 25, 30, 34, 38, 45, and 52 ms. To measure $\Delta R_2{}^*_{MION}$, GE EPI images were acquired before and after the same MION injection with TE = 10 ms.

BOLD and CBV-weighted fMRI data were acquired before and after injection of MION, respectively, from the same animals in which $\Delta R_{2\,MION}$ and $\Delta R_2{}^*_{MION}$ was measured. Echo times were chosen to maximize contrast-to-noise ratio (CNR) for each experiment; TE was 20 ms for GE BOLD fMRI, 40 ms for SE BOLD fMRI, 10 ms for GE CBV-weighted fMRI and 25 ms for SE CBV-weighted fMRI. For both GE BOLD and GE CBV-weighted fMRI studies, each run consisted of 10–**10**–10 image acquisitions (boldface represents stimulation on) with TR = 4 s. For both SE BOLD fMRI and SE CBV-weighted fMRI studies, 7–**5**–5 images were acquired with TR = 8 s. In preliminary low-resolution studies (in-plane resolution of 310 × 310 μm^2), CNR was ~1.5 times higher in GE compared to SE BOLD fMRI runs (see General Data Analyses section for computation, and see later for high-resolution studies). For similar CNRs, data were therefore averaged 3 times longer for SE vs. GE. Thus, a block of one GE run followed by 3 SE runs was repeated 10–20 times. Duration of SE and GE CBV-weighted fMRI studies was 3.0 ± 0.9 h (n = 5).

CBV-weighted SE fMRI at two echo times

Spin-echo EPI fMRI may have significant contributions from $\Delta R_2'$ (the difference between ΔR_2* and ΔR_2) when the readout time of EPI is relatively long compared to T_2* (Birn and Bandettini, 2002). This $\Delta R_2'$ contribution to spin-echo fMRI should be related to the data acquisition window and is independent of spin-echo times. To investigate TE-independent contributions to SE EPI fMRI, spin-echo times of 30 ms and 40 ms were interleaved in five animals after injection of MION, with TR for a single image = 2 s, and effective TR = 4 s for 2 TE images. Each run consisted of 10–**10**–10 image acquisitions. A total of 10–25 runs were obtained.

General data analyses

Signals from all fMRI runs under the same conditions were averaged. Then, data were processed using Stimulate (Strupp, 1996) and MATLAB routines (Mathworks, Natick, MA). Statistical t value maps were computed by comparing the experimental fMRI data acquired during control and stimulation periods on a pixel-by-pixel basis. To display fMRI maps, the statistical threshold was set to a t value of 2.0 ($P < 0.025$) and a minimum cluster size of 4 pixels was further imposed (Forman et al., 1995). Percentage signal change maps ($\Delta S/S$, where ΔS is the stimulation-induced signal change and S is the baseline signal intensity) were then calculated for statistically active pixels; images obtained during the pre-stimulus control period were considered as a baseline condition because post-stimulus fMRI signals did not quickly return to pre-stimulus signal

levels. Similarly, images acquired within the initial 8 s after onset of visual stimulation were not included due to a slow hemodynamic response. Our calculations assumed that $\Delta S/S$ values are linearly related to relaxation rate changes induced by stimulation, with zero intercept (i.e., $\Delta S/S = -\mathrm{TE}\cdot\Delta R_2$ in SE measurements, and $\Delta S/S = -\mathrm{TE}\cdot\Delta R_2{}^*$ in GE measurements). Color fMRI maps are overlaid on original baseline EPI images; increases in MRI signal intensities are displayed with hot colors (red/yellow), while decreases are shown in cold colors (blue/violet). Maximum and minimum values were chosen for display of image intensity levels; numbers shown at ends of each color or gray bar represent these limits. Graphs are plotted with standard errors of means (SEM), and all others are reported as mean ± standard deviation (SD).

Comparison between BOLD and CBV fMRI at high resolution

Baseline R_2 and R_2 changes induced by MION.* R_2 values were determined by fitting the logarithmic TE-dependent SE data to a linear function. $\Delta R_{2\ \mathrm{MION}}$ was calculated by subtraction of R_2 values without MION from those with MION. $\Delta R_2{}^*{}_{\mathrm{MION}}$ was calculated by $ln(S_{\mathrm{pre}}/S_{\mathrm{post}})/\mathrm{TE}$, where S_{pre} and S_{post} are signal intensities of control images (without any visual stimulation) before and after the injection of contrast agent, respectively.

Determination of relative CBV changes induced by stimulation. Stimulation-induced relaxation rate changes ($\Delta R_2{}^*{}_{\mathrm{stim}}$ and $\Delta R_2{}^*{}_{\mathrm{stim\ +\ MION}}$ for GE measurements without and with MION, and $\Delta R_{2\ \mathrm{stim}}$ and $\Delta R_{2\ \mathrm{stim\ +\ MION}}$ for SE measurements without and with MION, respectively) were calculated from the percentage signal changes as $-(\Delta S/S)/\mathrm{TE}$ for both BOLD and CBV-weighted studies under the assumption that the intravascular contribution is minimal. An increase in CBV decreases CBV-weighted fMRI signals, while a decrease in deoxyhemoglobin content increases fMRI signals. Consequently, a simultaneous BOLD response reduces the magnitude of CBV-weighted fMRI changes and must be removed from the stimulation-induced CBV-weighted response. With the assumption that the relaxation rate change induced by visual stimulation is linearly related to the product of cerebral blood volume and frequency shift of blood (Yablonskiy and Haacke, 1994; Kennan et al., 1998), the difference between stimulation-induced relaxation rate changes with MION (CBV-weighted) and without MION (BOLD) is related to the change in absolute CBV; $(\Delta R_2{}^*{}_{\mathrm{stim\ +\ MION}} - \Delta R_2{}^*{}_{\mathrm{stim}}) = k^*\cdot\Delta\mathrm{CBV}_{\mathrm{GE}}$, while $(\Delta R_{2\ \mathrm{stim\ +\ MION}} - \Delta R_{2\ \mathrm{stim}}) = k\cdot\Delta\mathrm{CBV}_{\mathrm{SE}}$, where $\Delta\mathrm{CBV}_{\mathrm{GE}}$ is the stimulation-induced total CBV change and $\Delta\mathrm{CBV}_{\mathrm{SE}}$ is the microvascular-weighted CBV change. Assuming that $\Delta R_2{}^*{}_{\mathrm{MION}}$ and $\Delta R_{2\ \mathrm{MION}}$ remain constant during measurements, baseline signal dependencies and BOLD contribution were removed from activation maps by calculating stimulation-induced changes in relative total CBV ($\Delta\mathrm{rCBV}_{\mathrm{total}}$) and changes in relative microvascular-weighted CBV ($\Delta\mathrm{rCBV}_{\mathrm{micro}}$), respectively (Kennan et al., 1998) as

$$\Delta\mathrm{rCBV}_{\mathrm{total}} = (k^*\cdot\Delta\mathrm{CBV}_{\mathrm{GE}})/(k^*\cdot\mathrm{CBV}_{\mathrm{GE}}) = (\Delta R_2{}^*{}_{\mathrm{stim+MION}} - \Delta R_2{}^*{}_{\mathrm{stim}})/\Delta_{R_2}{}^*{}_{\mathrm{MION}}, \quad (1)$$

$$\Delta\mathrm{rCBV}_{\mathrm{micro}} = (k\cdot\Delta\mathrm{CBV}_{\mathrm{SE}})/(k\cdot\mathrm{CBV}_{\mathrm{SE}}) = (\Delta R_{2\ \mathrm{stim+MION}} - \Delta R_{2\ \mathrm{stim}})/\Delta R_{2\ \mathrm{MION}}. \quad (2)$$

These $\Delta\mathrm{rCBV}_{\mathrm{total}}$ and $\Delta\mathrm{rCBV}_{\mathrm{micro}}$ values are quantitative and independent of TE, MION dose and BOLD contributions.

CNR and profile analyses. For quantitative analyses of high-resolution fMRI data, two quadrangular regions in area 18 within the visual cortex were independently selected (one within each hemisphere) based on T_1-weighted anatomical images (see Fig. 1A). Each region of interest (ROI) was 5–6 pixels wide along the dorsal flat surface of the cortex and ~11 pixels in the cortical depth dimension (perpendicular to the dorsal surface). These ROIs were placed along the dorsal part of the lateral gyrus near the medial end of the white matter at the position where the cortical curvature was least and where the variations of the cortical profile along the depth dimension were minimal. To calculate CNRs within the quadrangular ROIs, stimulation-induced signal changes and standard deviation of pre-stimulus baseline signals were determined on a pixel-by-pixel basis before any signal averaging. Then, CNR within the ROI was calculated for each animal by dividing the averaged stimulation-induced signal changes by the averaged standard deviation of baseline signal fluctuations, before averaging across all five animals. Additionally, CNR was calculated for all four experiments only for the pixels within the ROIs which were active in SE CBV-weighted fMRI.

To generate a signal profile in the cortical depth dimension, the average distance within quadrangular ROIs from the surface of the cortex to the gray/white matter boundary was determined in each animal. Data were then spatially interpolated with the linear nearest-neighbor resampling method (Tsao, 2003) to 22 pixels, resulting in an average depth resolution of ~78 μm. Then the signals at the same relative cortical depth, regardless of statistical criteria for activation, were averaged along the surface dimension. One profile was generated for each animal from the quadrangular ROIs in area 18. Cortical layer locations were assigned based on relative distances of those layers in area 18 (Payne and Peters, 2002). From the cortical depth profiles of percentage changes for CBV-weighted fMRI and relative CBV, values were calculated for peak position, full width at half maximum (FWHM) and peak intensity.

CBV-weighted SE fMRI at two echo times

Data were zero-padded to matrix size = 128 × 128. To quantitatively determine stimulation-induced TE-independent contributions to CBV-weighted SE fMRI, cerebral spinal fluid (CSF) and cortical ROIs were selected. Areas outside the cortical surface which contain both CSF and large cortical surface vessels were defined from high-intensity areas on pre-MION T_2 maps; pixels which were commonly activated within these areas at both TE values were assigned to be CSF ROIs. In these low-resolution studies, it is difficult to accurately select quadrangular ROIs as defined in high-resolution studies; therefore, approximately 500 pixels with the highest t values averaged over maps from both TE values were assigned to represent cortical ROIs. Percentage changes of ROI-averaged signals were linearly fitted against the TE values.

Results

Basal SE and GE CBV distributions obtained from R_2 and R_2 changes*

To determine the relationship between baseline blood volume and functional activity, the distribution of CBV values across the cortex was determined from relaxation rate changes induced by

contrast agent without any visual stimulation. Fig. 1 shows illustrative data from one animal. Anatomical boundaries between gray and white matter were determined by a T_1-weighted EPI image (Fig. 1A). The dorsal part of the lateral gyrus is visual area 18 (Payne and Peters, 2002), and the medial section of the lateral gyrus is area 17. The two quadrangular ROIs defined within visual area 18 for subsequent cortical depth-dependent analysis are shown in Fig. 1A. The average thickness of these quadrangular ROIs is 1.67 ± 0.07 mm (n = 5 animals). Basal T_2 values (Fig. 1B) are the highest (~70 ms) outside the cortical surface where cerebral spinal fluid (CSF) resides (indicated by the green contours), and decrease to ~40 ms in the cortex.

The area where total CBV (linearly dependent on $\Delta R_2{}^*_{\mathrm{MION}}$) is highest (bright color in Fig. 1C) is mainly located near the surface of the cortex. In some areas, intracortical penetrating vessels are also detectable as indicated by red arrows. In contrast, parenchymal signal in microvascular-weighted CBV (dependent on $\Delta R_{2\ \mathrm{MION}}$) is maximal at the middle cortical layers (Fig. 1D), which is consistent with previous findings that middle cortical layers have the highest microvascular density (Tieman et al., 2004). Rather unexpectedly, $\Delta R_{2\ \mathrm{MION}}$ values are also relatively large at the cortical surface (see Discussion). An interesting observation from within the large CSF area between the two hemispheres is that changes within the central portion (indicated by the yellow arrow) are very small after MION administration, because this region is devoid of vessels.

Comparison of BOLD and CBV-related responses to visual stimulation at high resolution

BOLD and CBV-weighted fMRI induced by visual stimulation were obtained with GE (Figs. 2A and C) and SE (Figs. 2B and D) data acquisitions before (BOLD; Figs. 2A and B) and after (CBV-weighted; Figs. 2C and D) MION injection. In conventional GE BOLD fMRI (Fig. 2A), signal intensities increased during visual stimulation, indicating an increase in venous oxygenation; the highest percentage signal changes (yellow pixels) were seen in the CSF space (within the green contours), where pial veins are located. This observation is consistent with our previous GE BOLD studies at 9.4 T (Duong et al., 2000b; Zhao et al., 2004a). The large vessel contribution to BOLD signals is reduced using SE BOLD fMRI (Fig. 2B) because the dephasing around large vessels refocuses, thus contributing less to the fMRI signal changes (Ogawa et al., 1993). These results are consistent with previous 9.4 T SE BOLD observations (Lee et al., 1999; Zhao et al., 2004a). In both GE and SE BOLD maps, high signal changes (yellow) also appear within the cortex.

Signal intensities of CBV-weighted fMRI decreased during visual stimulation (blue/violet), indicating an increase in CBV.

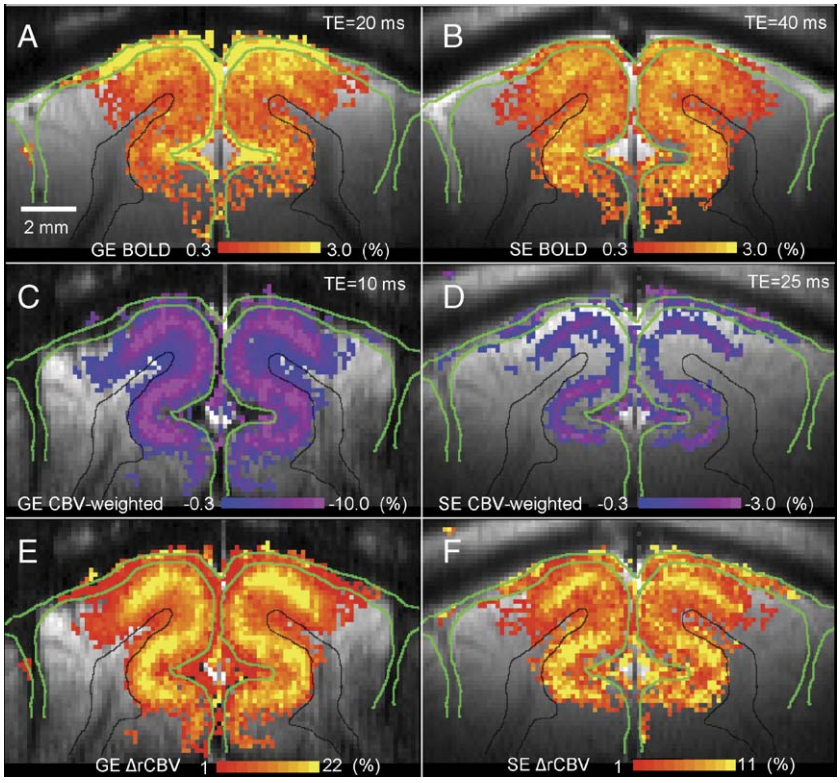

Fig. 2. Comparison of BOLD and CBV-related responses to visual stimulation. Visual stimulation-induced BOLD (A, B) and CBV-weighted fMRI data (C, D) of the same animal as shown in Fig. 1 were obtained before (BOLD) and after (CBV-weighted) injection of 10 mg Fe/kg MION, and are displayed as percentage signal changes. Positive $\Delta S/S$ changes (red/yellow) are observed in GE (TE = 20 ms) and SE BOLD fMRI (TE = 40 ms) (A and B, respectively), while negative $\Delta S/S$ changes (blue/violet) are detected in GE (TE = 10 ms) and SE CBV-weighted fMRI (TE = 25 ms) (C and D, respectively), indicating an increase in CBV. Peaks of CBV responses are localized to the middle of the cortex. (E, F) Quantitative GE and SE ΔrCBV responses to visual stimulation were calculated by taking into account the BOLD contribution and normalizing with baseline CBV distributions on active pixels in either BOLD or CBV weighted fMRI (see Eqs. (1) and (2), respectively). Quantitative rCBV changes in response to neural activity are therefore independent of deoxyhemoglobin changes and contrast agent concentrations. GE and SE rCBV changes are also maximal near the middle of the cortex.

Significant signal changes were detected near the cortical surface in both GE (Fig. 2C) and SE (Fig. 2D) CBV-weighted fMRI, which might be due to propagated upstream vasodilation (Iadecola et al., 1997). When the statistical threshold was reduced, we sometimes observed CBV changes that followed along the intracortical vessels (data not shown), suggesting that both pial and penetrating vessels dilate. However, in both GE (Fig. 2C) and SE (Fig. 2D) CBV-weighted maps, the highest signal changes (violet pixels) followed the middle of the visual cortex. In all five animals, similar BOLD and CBV-weighted fMRI results were observed.

To compare the sensitivity of four different fMRI techniques, CNRs (i.e., stimulation-induced signal changes divided by average pixel-wise baseline fluctuations) were determined within the quadrangular ROIs (Fig. 1A). CNRs were 0.54 ± 0.27 and 0.43 ± 0.13 (n = 5 animals) for GE and SE BOLD fMRI, respectively; CNRs were 0.81 ± 0.22 and 0.28 ± 0.04 for GE and SE CBV-weighted fMRI, respectively. To determine CNRs in the middle of the cortex, only active pixels in SE CBV-weighted fMRI (Fig. 2D) within quadrangular ROIs were selected for analysis; CNRs were then 0.52 ± 0.30 and 0.50 ± 0.19 (n = 5) for GE and SE BOLD fMRI, respectively; CNRs were 1.29 ± 0.40 and 0.50 ± 0.04 (n = 5) for GE and SE CBV-weighted fMRI, respectively. These data indicate that CBV-weighted GE studies are more sensitive than corresponding SE measurements. Relatively low sensitivity in all high-resolution fMRI studies requires extensive signal averaging.

To remove the dependency of the MION dose and to take into account the BOLD contribution to CBV-weighted fMRI, quantitative GE and SE rCBV change (ΔrCBV) maps in response to visual stimulation (Figs. 2E and F) were obtained from corresponding active pixels in either BOLD or CBV-weighted fMRI. The activation patterns within the quantitative ΔrCBV maps (Figs. 2E, F) mirror those of CBV-weighted fMRI maps (Figs. 2C, D); the highest GE and SE rCBV changes (yellow pixels in Figs. 2E, F) follow near the middle cortical layers, which is consistent with findings of hemodynamic-based imaging studies (Mandeville and Marota, 1999; Duong et al., 2000b; Harel et al., 2002b; Lu et al., 2004) and 2-deoxyglucose metabolism studies (Kennedy et al., 1976; Woolsey et al., 1996).

Average cortical depth profiles

Profiles of signal changes across cortical layers were obtained from the two quadrangular ROIs within area 18 (outlined in red in Fig. 1A). Averages of results from five animals were plotted as a function of depth from the surface of the cortex (Fig. 3). Baseline CBV_{GE} without visual stimulation ($\Delta R_2{}^*_{MION}$, squares in Fig. 3A) is highest at the cortical surface, and decreases with depth. In contrast, baseline CBV_{SE} ($\Delta R_{2\ MION}$, circles in Fig. 3A) is maximal at 0.86 ± 0.11 mm depth (n = 5). The average $\Delta R_2{}^*_{MION}$ and $\Delta R_{2\ MION}$ values in the cortical ROI are 65.3 ± 9.8 s^{-1} and 14.2 ± 3.5 s^{-1} (n = 5), respectively.

In GE BOLD fMRI (squares in Fig. 3B), large signal changes are observed in upper cortical layers (layers 1–3) due to the magnetic susceptibility effect from large surface vessels. In both SE and GE BOLD profiles, signal differences between other layers are small, with only a low intensity peak observed within lower and/or middle cortical layers. The general cortical pattern of GE BOLD signal changes is similar to that of baseline total CBV ($\Delta R_2{}^*_{MION}$), and differs from that of microvascular-weighted CBV ($\Delta R_{2\ MION}$). Average $\Delta R_2{}^*_{stim}$ and $\Delta R_{2\ stim}$ values in the cortical ROI are −0.62 ± 0.29 s^{-1} and −0.23 ± 0.11 s^{-1} (n = 5),

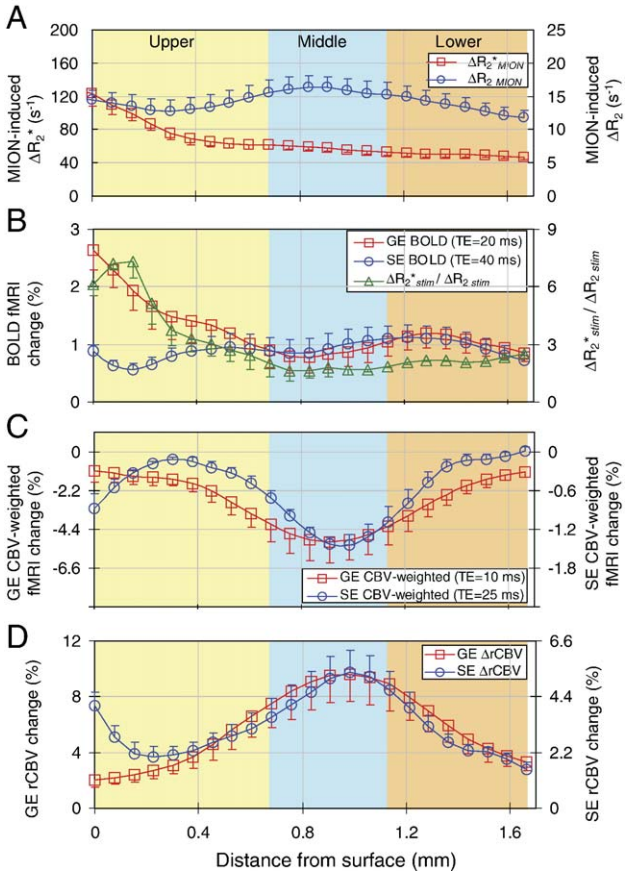

Fig. 3. Average cortical depth profiles. One profile was generated for each animal from the quadrangular ROIs in area 18 (e.g., Fig. 1A), then data were averaged across all five animals. The surface of the cortex is at zero, with cortical depth represented by increasing distances. Approximate location of cortical layers was determined by relative distances of those layers in area 18 (Payne and Peters, 2002) and is differentiated by colored bands; middle cortical layer (approximately layer 4) is located in the region between 0.7 mm to 1.15 mm from the surface of the cortex. Red squares indicate GE data points, while blue circles indicate SE data points. (A) Cortical depth profiles without visual stimulation obtained from MION-induced signal changes reflect the distribution of total CBV ($\Delta R_2{}^*_{MION}$, squares) and microvascular-weighted CBV signals ($\Delta R_{2\ MION}$, circles). The area with largest CBV_{GE} is located at the surface of the cortex, while the region of highest CBV_{SE} is located within the middle cortical layer. (B) For both GE BOLD fMRI (squares) and SE BOLD fMRI (circles), the percentage signal changes are positive, indicating an increase in venous oxygenation. The ratio of $\Delta R_2{}^*_{stim}$ to $\Delta R_{2\ stim}$ (triangles) is larger in the upper cortical layer than in the middle and lower cortical layers. (C) For both GE CBV-weighted fMRI (squares) and SE CBV-weighted fMRI (circles), the $\Delta S/S$ changes are negative, indicating an increase in CBV. (D) Changes in both total rCBV (squares) and microvascular-weighted rCBV (circles) peak at ~1 mm depth, similar to both GE and SE CBV-weighted fMRI data. For clarity, only one side of the error bars (SEM) is shown.

respectively, which is consistent with our previous observation (Zhao et al., 2004a). Since the ratio of $\Delta R_2{}^*_{stim}$ to $\Delta R_{2\ stim}$ is related to the size of vessels responding to BOLD fMRI, a profile of the ratio ($\Delta R_2{}^*_{stim}/\Delta R_{2\ stim}$) across cortical layers is also shown in Fig. 3B. Since there is minimal intravascular signal due to the short T_2 of venous blood at 9.4 T, we can interpret our results according to simulations of the extravascular BOLD effect. Previous simulations have shown that for a frequency shift of 40

Hz and a vessel radius of <5 μm, $\Delta R_2{}^*_{stim}/\Delta R_{2\ stim}$ should be <2.5 (Fig. 6 in (Ogawa et al., 1993)); our values for $\Delta R_2{}^*_{stim}/\Delta R_{2\ stim}$ are even smaller within middle and lower cortical layers, suggesting that microvascular contributions dominate the 9.4 T BOLD fMRI signals in these regions.

Unlike BOLD signals, the largest CBV-weighted fMRI signals (Fig. 3C) and rCBV changes (Fig. 3D) occur at the middle cortical area. Average ($\Delta R_2{}^*_{stim\ +\ MION} - \Delta R_2{}^*_{stim}$) and ($\Delta R_{2\ stim\ +\ MION} - \Delta R_{2\ stim}$) in the cortical ROI were 3.44 ± 1.77 s^{-1} and 0.46 ± 0.11 s^{-1} (n = 5), respectively. Quantitative values for peak position, FWHM, and peak intensity of CBV-related fMRI responses are given in Table 1. Peak positions for all CBV fMRI profiles are located ~1 mm from the cortical surface. All of the functional FWHMs are <1 mm, and FWHMs of SE are narrower than those of GE. It should be noted that FWHMs were overestimated for both GE and SE data because of blurring effects along the phase-encoding (dorsal–ventral) direction.

CBV-weighted SE fMRI at two echo times

To investigate whether the SE fMRI signal change is affected by factors other than ΔR_2, CBV-weighted data were obtained both with TE = 30 ms (Fig. 4A) and TE = 40 ms (Fig. 4B). Similar to high-resolution maps (Fig. 2D), the highest parenchymal signal changes (violet pixels) followed the middle of the visual cortex. A linear fit of SE CBV-weighted fMRI percentage changes vs. TE values yields a slope which represents $-\Delta R_{2\ stim\ +\ MION}$ and an intercept which represents the TE-independent component, which includes $\Delta R_2'$ and inflow effects. Pixel-by-pixel analysis was replaced by ROI analysis due to the limited sensitivity of these multiple-TE studies. Within the CSF ROI (pink pixels on inset superimposed in Fig. 4A), averaged $\Delta R_{2\ stim\ +\ MION}$ and intercept values are 0.34 ± 0.20 s^{-1} and −0.0009 ± 0.0052 (n = 5); within the cortical ROI (pink pixels on inset superimposed in Fig. 4B), averaged $\Delta R_{2\ stim\ +\ MION}$ and intercept values are 0.32 ± 0.24 s^{-1} and −0.0011 ± 0.0047 (n = 5). Peak cortical values for CBV-weighted fMRI percentage change divided by TE in high-resolution studies (GE vs. SE CBV-weighted values in Table 1) are −0.0529/0.010 s^{-1} vs. −0.0153/0.025 s^{-1}, giving a $\Delta R_2{}^*_{stim\ +\ MION}/\Delta R_{2\ stim\ +\ MION}$ ratio of ~8.6. If we assume that similar changes occur in these multiple TE studies, then expected $\Delta R_2{}^*_{stim\ +\ MION}$ values are ~2.94 s^{-1} for active pial vessel areas within CSF and ~2.75 s^{-1} for the cortex. As a very simplistic, but reasonable approximation, if there is a 10% contribution from $\Delta R_2{}^*_{stim\ +\ MION}$ to the SE fMRI signal during the readout time of 34 ms, then the intercept due to the $\Delta R_2'$ contribution should be >0.0100 for pial vessels in CSF and >0.0094 for the cortex, considerably more than our results show. Our intercepts are not significantly different from zero ($P < 0.05$), indicating that any contributions to the SE CBV-weighted fMRI signal other than ΔR_2 are negligible. It should be noted that the data acquisition window for this single-shot EPI data is longer than that of the four-shot high-resolution EPI data (~41 ms vs. ~34 ms).

Table 1
Quantification of cortical depth-dependent CBV fMRI responses[a]

	Peak position[b] (mm)	FWHM (mm)[c]	Peak intensity (%)[d]
GE CBV-weighted change	0.94 ± 0.03	0.81 ± 0.07	−5.29 ± 2.56
SE CBV-weighted change	0.96 ± 0.06	0.52 ± 0.02	−1.53 ± 0.25
GE ΔrCBV	1.00 ± 0.09	0.92 ± 0.09	9.96 ± 4.12
SE ΔrCBV	1.00 ± 0.08	0.79 ± 0.14	5.55 ± 1.80

[a] CBV-weighted fMRI changes induced by visual stimulation were obtained using GE and SE imaging techniques after the injection of MION. Quantitative GE and SE relative CBV changes (ΔrCBV) were determined from GE and SE CBV-weighted fMRI, respectively, after the correction for BOLD contamination and normalization of baseline blood volume. Cortical depth profiles within the quadrangular ROIs in area 18 (see Fig. 1A) were obtained for each study (see Fig. 3 for the averaged profiles), and peak position, full width at half maximum (FWHM), and peak intensity were individually calculated, then averaged for mean ± SD tabulation (n = 5 animals).

[b] Peak position is distance from the cortical surface. Total cortical thickness within ROIs is 1.67 ± 0.07 mm (n = 5). Based on literature (Payne and Peters, 2002), layer 4 is located in the region between approximately 0.7 mm and 1.15 mm from the surface of the cortex.

[c] Measured FWHM is artificially broadened by T_2* (apparent transverse relaxation time) decay during data acquisition and therefore overestimated.

[d] Peak intensity of GE ΔrCBV and SE ΔrCBV without the BOLD correction is 8.97% and 3.64%, respectively.

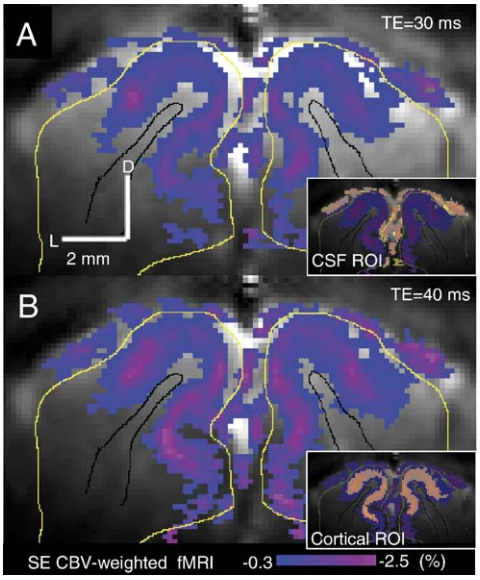

Fig. 4. CBV-weighted SE fMRI at two echo times. Spin-echo times of 30 ms (A) and 40 ms (B) were used to determine contributions other than ΔR_2 to CBV-weighted SE fMRI. A T_1-weighted anatomical image appears in the background with the cortical surface outlined in yellow contours and white matter boundaries delineated by black contours. Quantitative analysis was conducted within the pink pixels indicated in inset images for the CSF ROI (A) and the cortical ROI (B). D: dorsal, L: lateral.

Discussion

Basal GE and SE CBV distribution

The R_2* changes induced by MION ($\Delta R_2{}^*_{MION}$) are considered to be an index of total blood volume (Boxerman et al., 1995; Tropres et al., 2001). This is valid only when the signal intensity of pixels is not influenced by static magnetic susceptibility effects from neighboring pixels. In our high-resolution images with in-plane resolution of 156 × 156 μm^2, $\Delta R_2{}^*_{MION}$ monotonically decreased with cortical depth, especially in the region near the

surface, which may be partly due to susceptibility effects from large surface vessels. By comparison, the R_2 changes induced by MION ($\Delta R_{2\ \mathrm{MION}}$) are considered to be an index of microvascular-weighted blood volume (Boxerman et al., 1995; Tropres et al., 2001), assuming that the diffusion coefficients of water are similar across pixels (Kennan et al., 1994; Boxerman et al., 1995). In our studies, it is reasonable to ignore intravascular contributions at 9.4 T since the cortical baseline R_2 value of ~25 s^{-1} increased after MION injection to ~39 s^{-1}, resulting in a signal reduction of ~57% in images with TE = 40 ms; this signal reduction must therefore be dominated by extravascular contributions, because changes due to intravascular contributions must be ≤5% at 9.4T (van Zijl et al., 1998; Lee et al., 1999). Our results show maximal $\Delta R_{2\ \mathrm{MION}}$ values at the middle cortical layers, but also relatively large values at the cortical surface. According to analytical solutions (Tropres et al., 2001; Kiselev et al., 2005), in the static dephasing domain (i.e., TE × frequency shift induced by MION >> 1), $\Delta R_{2\ \mathrm{MION}}$ (see Eq. (9) in (Kiselev et al., 2005)) is described as:

$$\Delta R_{2\ \mathrm{MION}} = c \times CBV \times D^{1/3} \times R^{-2/3} \quad (3)$$

where c is the constant related to the frequency shift induced by MION, CBV is the blood volume, D is the diffusion coefficient, and R is the weighted-mean radius of vessels. Near the surface of the cortex, the diffusion coefficient of CSF is 3 times larger than that of parenchyma (Annet et al., 2002). An index of CBV can be obtained from $\Delta R_2{}^*{}_{MION}$; CBV at the surface of the cortex appears >2 times higher than within the parenchyma (see Fig. 1C and red squares in Fig. 3A). Assuming that the weighted-mean vessel radius is 5 μm in the parenchyma (Tropres et al., 2001) and 25 μm in the CSF area, $\Delta R_{2\ \mathrm{MION}}$ in the CSF region can be as high as $\Delta R_{2\ \mathrm{MION}}$ within parenchyma. This analysis suggests that $\Delta R_{2\ \mathrm{MION}}$ values are only valid for quantification of microvascular-weighted CBV distribution within the parenchyma. A similar argument applies to $\Delta R_{2\ \mathrm{stim}}$ and $\Delta R_{2\ \mathrm{stim\ +\ MION}}$ values in fMRI data.

TE-independent contributions to SE-EPI fMRI signals

In SE fMRI studies performed at multiple TE values, existence of TE-independent contributions should be detectable as a non-zero intercept of a linear fit of percentage signal change vs. TE. Factors not related to TE (i.e., unrelated to ΔR_2), include inflow contributions, intravascular sources and $\Delta R_2'$. Since T_2' effects are greatest for high k-space lines acquired at the edge of the readout time, the largest $\Delta R_2'$ effect is likely to appear in high-frequency components, such as the edge of functionally-active regions or finely-detailed structures like the cortical surface. However, in our SE CBV-weighted fMRI studies performed at two TE values, both the CSF and cortical ROI intercepts are negligible, suggesting that overall TE-independent contributions are minimal. Contributions from inflow and intravascular signals are negligible in CBV-weighted fMRI because of the short T_2 blood values induced by MION; thus the $\Delta R_2'$ contribution to CBV-weighted SE fMRI must also be negligible. Since a $\Delta R_2'$ contribution to CBV-weighted SE fMRI was not detected, this contribution to SE BOLD fMRI might also be expected to be minimal. This expectation is consistent with our lab's TE-dependent SE BOLD fMRI studies (Jin et al., 2005) and previous SE BOLD studies at 7 T (Yacoub et al., 2003): when the contribution from intravascular signal and inflow is minimized by the application of diffusion-weighted gradients (in the absence of MION), the intercept is zero, indicating that the $\Delta R_2'$ contribution to SE BOLD fMRI is negligible, although the reason for these findings is not clear.

Biophysical aspects of CBV-weighted fMRI responses

In the brain mapping community, statistical values have been commonly used to detect peaks of activation foci. Statistical values are closely correlated with stimulation-induced changes in absolute signals; higher absolute signal changes from baseline signal intensities (ΔS) result in higher statistical values. After the injection of contrast agent, the baseline signal intensity ($S_{\mathrm{post\text{-}MION}}$) is related to TE and the MION concentration; thus, the choice of TE value and MION dose can alter the spatial distribution and intensity of absolute signal changes (or t values) in CBV-weighted fMRI (Mandeville and Marota, 1999). Similar arguments can be applied to BOLD measurements because baseline signal intensities are dependent on imaging techniques and parameters. To remove these baseline signal dependencies from the activation maps, we determined percentage signal changes from baseline ($\Delta S/S$) for all BOLD and CBV-weighted maps and profile analyses.

$\Delta S/S$ maps of CBV-weighted fMRI still contain contributions from changes in deoxyhemoglobin contents (i.e., BOLD) (see Materials and methods) and therefore the spatial distribution and intensities within these maps still may not be true representations of CBV changes. Our CBV data showed that peak positions of ΔrCBV were similar to $\Delta S/S$ (Table 1). This indicates that the BOLD contribution to CBV-weighted fMRI is either relatively small, or else spatially homogeneous across the cortex. Indeed, the BOLD contribution to SE CBV-weighted fMRI is spatially homogeneous, but quite significant (see Fig. 3B circles with TE = 40 ms vs. Fig. 3C circles with TE = 25 ms), while the BOLD contribution to GE CBV-weighted fMRI is considerably smaller (see Fig. 3B squares with TE = 20 ms vs. Fig. 3C squares with TE = 10 ms). Even with our experimental conditions, which fortuitously minimized the effective contribution of BOLD to the CBV-weighted peak position, the peak intensity and FWHM were still dependent on the change in deoxyhemoglobin contents (BOLD). The BOLD contribution was removed by subtracting $\Delta R_2{}^*{}_{\mathrm{stim}}$ from $\Delta R_2{}^*{}_{\mathrm{stim\ +\ MION}}$ (for GE) or $\Delta R_{2\ \mathrm{stim}}$ from $\Delta R_{2\ \mathrm{stim\ +\ MION}}$ (for SE), where it is assumed that the intravascular contribution to BOLD signals is minimal and that the relaxation rate change induced by visual stimulation is linearly related with frequency shift of blood (Kennan et al., 1998). The former assumption is reasonably valid because T_2 and $T_2{}^*$ values of venous blood at 9.4 T are relatively short compared to the TE values. The latter assumption may not be valid in spin-echo measurements (Kiselev and Posse, 1999); in this case, our BOLD correction may over-compensate and thus our BOLD-corrected ΔrCBV values are likely to be upper estimates of the real changes. Further in vivo studies are required to address this question.

The BOLD contribution to CBV-weighted fMRI could also be minimized by using an extremely short TE value and a large dose of MION. However, a high dose of contrast agent reduces $T_2{}^*$ of blood and surrounding tissue, and thus it is difficult to acquire high-quality images using fast imaging techniques. In our studies, a dose of 10 mg Fe/kg was chosen to give sufficient CBV contrast with high-resolution EPI images (Kim and Ugurbil, 2003); the improvement of CNR in GE fMRI was 1.5-fold (0.81 in CBV-weighted fMRI vs. 0.54 in BOLD fMRI). This enhancement is consistent with that of 1.2-fold found in our previous low-resolution 9.4 T studies (10 mg Fe/kg dose, TE = 15 ms for

CBV-weighted fMRI vs. TE = 20 ms for BOLD fMRI) (Zhao et al., 2003). Very recently, Mandeville et al. (2004) reported that CNR in CBV-weighted GE fMRI with 28 mg Fe/kg and TE of 5 ms was improved 2-fold compared to GE BOLD with TE of 10 ms in rat brain during cocaine stimulation.

After the BOLD contribution to CBV-weighted fMRI is corrected, baseline signal dependencies must be removed for the quantification of rCBV changes (see Eqs. (1) and (2)). In our studies, constant baseline signal intensity was assumed. However, baseline signal intensities (without stimulation) increased over time due to the washout of MION during relatively long fMRI studies (~3 h), introducing ΔrCBV quantification errors. To evaluate this, the average change in baseline signals during all fMRI runs with MION was determined by $ln(S_1/S_2)/TE$, where S_1 and S_2 are the averaged baseline signal intensities of the first and second half of fMRI trials, respectively. The change to baseline ΔR_2 due to washout of MION in blood ($\Delta R_{2\ washout}$) is $-0.6 \pm 0.5\ s^{-1}$ ($n = 5$) within the two quadrangular ROIs, which in turn creates an underestimation of the $\Delta rCBV_{micro}$ value by 4.4% (i.e., $\Delta R_{2\ MION} / (\Delta R_{2\ MION} - \Delta R_{2\ washout}) = 14.2 / (14.2-0.6) = 1.044$). Since data acquisition for GE and SE was interleaved, average percent errors of $\Delta rCBV_{total}$ and $\Delta rCBV_{micro}$ values should be similar. Due to poor SNR of each fMRI run, we did not attempt to correct variations of baseline signal intensities on a pixel-by-pixel basis or on a run-by-run basis.

Spatial specificity of SE CBV-weighted fMRI

In SE CBV-weighted fMRI maps (Fig. 2D), the localized signal change was mostly observed at the middle of the cortex. This appearance may be caused by the relatively low sensitivity of SE CBV-weighted fMRI when a relatively high statistical threshold is used. To evaluate this, raw stimulation-induced subtraction maps (ΔS, Fig. 5A) were determined (without any threshold applied) as the difference between images acquired during stimulation vs. pre-stimulus control. Also, a low-threshold statistical t value map ($t \geq |1.5|$, no clustering applied, $P \leq 0.2$) was calculated (Fig. 5B). Most pixels within the upper and lower cortical regions show changes similar to the noise regions, while at the middle of the cortex, the t value was <-15. This suggests that the high specificity at the middle of the cortex is not due to poor sensitivity of SE CBV-weighted fMRI. This conclusion was also supported by the profile analysis where no statistical threshold was applied (see Fig. 3C). However, the high spatial specificity of SE CBV-weighted fMRI does not necessarily mean that the microvascular CBV response has higher spatial specificity than the total CBV response. From Figs. 2E–F and 3D, it can be seen that the spatial profile of microvascular rCBV response is actually similar to that of total rCBV. These results merely reflect the larger contribution of the SE BOLD signal to SE CBV-weighted fMRI as compared to the GE BOLD effect in GE CBV-weighted fMRI.

rCBV change vs. SE BOLD fMRI

SE BOLD changes result from oxygenation increases mostly in venous microvessels (see circles in Fig. 3B), while SE and GE rCBV changes are due to volume changes in arterial and venous vessels (see circles and squares in Fig. 3D). If an oxygenation level change is correlated with a change in vascular volume (as is commonly assumed), then spatial responses across the cortex should be similar. However, this is not our observation, and the data is most likely explained by sources of BOLD signals which are not clearly understood. The SE BOLD signal may have reduced spatial specificity due to contributions from intravascular spins, but CBV-weighted fMRI does not have intravascular contributions because of the short T_2 blood values induced by MION. The extravascular BOLD signal is related to baseline venous blood volume and its change, and to the change in venous oxygenation from the mismatch between the CBF and $CMRO_2$ increases (Ogawa et al., 1998). The profile of BOLD signals is therefore dependent on baseline blood volume distribution and cortical depth-dependent stimulation-induced changes in CBF, $CMRO_2$, and venous CBV. These complex biophysical mechanisms can explain the observed difference between SE BOLD vs. SE and GE ΔrCBV responses. Our SE BOLD observation at 9.4 T cannot be easily extrapolated into 1.5 T and 3.0 T SE BOLD studies because the intravascular contribution is significant at low magnetic fields, further reducing the spatial specificity (Oja et al., 1999).

Detection of laminar-dependent CBV regulation

The cortical vascular system is constructed of relatively large pial vessels, where generally the arteries penetrate and the veins emerge from the cortex perpendicular to its surface. Penetrating arteries with an inter-vessel distance of ~250 μm (Mchedlishvili and Kuridze, 1984) extend hundreds of microns deep into the cortical tissue, branch out into arterioles and eventually connect to capillary mesh with an inter-capillary distance of ~24 μm (Pawlik

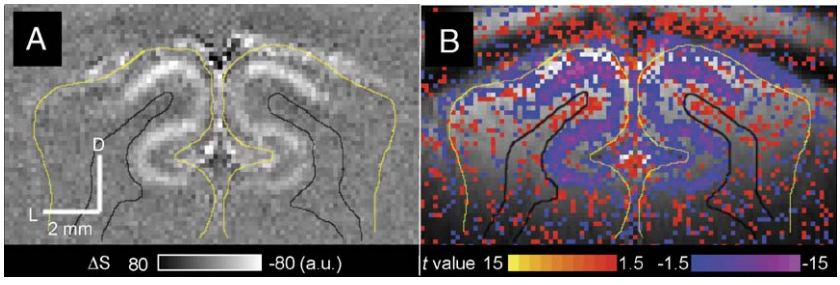

Fig. 5. Spatial specificity of SE CBV-weighted fMRI. Raw gray-scale functional map of SE CBV-weighted fMRI (A) was determined without any threshold by subtraction of images obtained during pre-stimulus control from those obtained during stimulation; data is from the same animal shown in Figs. 1 and 2. The bright pixels have the largest (most negative) signal changes induced by stimulation. D: dorsal, L: lateral, a.u.: arbitrary unit. Statistical t value map (B) was obtained using a t value threshold of -1.5 (no clustering applied, $P \leq 0.2$). The most significant stimulation-induced signal changes appear in the middle cortical layer. The yellow contours which outline the cortical surface and the black contours which delineate the white matter were obtained from the T_1-weighted anatomical image and then superimposed on A and B.

et al., 1981). Our data can help to determine the size of vessels which have blood volume changes in response to neural stimuli, and thus, providing insight into CBV regulation.

The diameter of penetrating arteries and emerging veins is smaller at deeper cortical regions, and also some arteries/veins extend only to the upper cortical layers (Duvernoy et al., 1981). Thus, if CBV changes during stimulation are dominated by dilation of penetrating arteries, then the CBV increase in the upper cortical layer should either exceed or be similar to that in the middle cortical layer. However, CBV responses in our data were not evenly distributed across cortical layers and in fact were highest at the middle cortical region. This suggests that dilation of intracortical vessels is not the major source of CBV change, and that volume of "downstream" vessels increases during stimulation. If "downstream" vessels passively dilate across cortical layers in response to dilation of "parent" intracortical arteries, and if the relative distribution of different-sized vessels is similar across cortical layers, then a CBV change will follow the baseline CBV distribution. Under this condition, even though the highest absolute CBV change can occur at the middle cortical layer, the relative CBV change normalized by the baseline volume (ΔrCBV) is expected to be constant across cortical layers. However, this is not the case in our findings (see Fig. 3D), suggesting that a finer active control mechanism exists at a "downstream" vascular level and/or that the relative ratio of vessel sizes undergoing volume change is heterogeneous across the cortex.

Our observation in the middle cortical layer shows that microvascular-weighted blood volume changes (5.6%, obtained from SE) are less than total blood volume changes (10%, obtained from GE). To explain our SE and GE CBV observations by means of vessel-size dependent responses, parenchymal vessels are assumed to be divided into two groups, micro- and macro-vessels, based on the detection ability of the SE-weighted MRI technique (see also Introduction). Baseline $CBV_{GE} = CBV_{micro} + CBV_{macro}$ where CBV_{micro} and CBV_{macro} is the micro- and macro-vascular volume, respectively. Since a portion of small arterioles and venules can contribute to these SE measurements, the boundary between micro- and macro-vessels is not well defined. But even conservatively, capillaries belong to the microvascular group, while intracortical and relatively large "branching" vessels belong to the macrovascular group. Changes in relative total and microvascular volumes were measured in our studies, where stimulation-induced $\Delta rCBV_{total} = (\Delta CBV_{micro} + \Delta CBV_{macro}) / (CBV_{micro} + CBV_{macro})$ while $\Delta rCBV_{micro} = \Delta CBV_{micro} / CBV_{micro}$. If a change in intracortical and relatively large "branching" vessels is dominant, then $\Delta rCBV_{micro}$ (measured by SE fMRI) should be very small, as compared to $\Delta rCBV_{total}$ (measured by GE fMRI). If a change in capillary volume is dominant, $\Delta rCBV_{micro}$ should be larger than $\Delta rCBV_{total}$. If CBV increases are similar in all sizes of vessels, then $\Delta rCBV_{micro}$ should be similar to $\Delta rCBV_{total}$. Our data do not support any of these possibilities, suggesting that the CBV change is not uniform for all sizes of vessels, and that the dominant changes occur in vasculature with diameters larger than capillaries, but smaller than intracortical vessels.

Vessel-size dependent CBV regulation

Insight into mean vessel sizes can be obtained from combined gradient-echo and spin-echo data after the injection of contrast agents (Dennie et al., 1998; Jensen and Chandra, 2000; Tropres et al., 2001, 2004; Wu et al., 2004; Kiselev et al., 2005). With a frequency shift in plasma of ~300 Hz after administration of a 10-mg Fe/kg dose of MION (Zhao et al., 2003), the maximal sensitivity of SE MRI occurs for vessels with a radius of 1–2 μm, and then decreases for larger-size vessels as shown in Eq. (3)

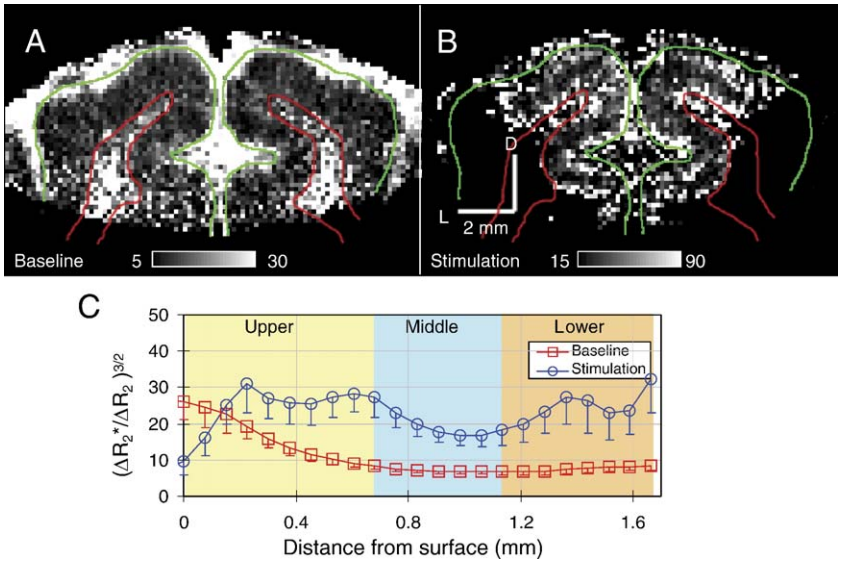

Fig. 6. Baseline and stimulation relative vessel size indices. (A) Relative VSI during the baseline condition shows a comparatively high ratio of large to small vessels at the cortical surface and within white matter; this map was generated by calculating $(\Delta R_2{}^*_{MION}/\Delta R_{2\ MION})^{3/2}$ values from the data of Figs. 1C and 1D. (B) Relative VSI during stimulation shows that in the middle of the cortex more of the small vs. large vessels are contributing to the CBV change due to neural activity than in the lower cortical region; this map was generated by calculating $((\Delta R_2{}^*_{stim\ +\ MION} - \Delta R_2{}^*_{stim})/(\Delta R_{2\ stim\ +\ MION} - \Delta R_{2\ stim}))^{3/2}$ values from the stimulation data of Figs. 2A–D. D: dorsal, L: lateral. (C) Profiles of relative VSI values during baseline and stimulation conditions from the quadrangular ROIs in area 18 (e.g., Fig. 1A) were generated for each animal, then data were averaged across all five animals (similar analysis method to that of Fig. 3). Generally, stimulation relative VSI values (circles) are higher than baseline relative VSI values (squares). For clarity, only one side of the error bars (SEM) is shown.

(Ogawa et al., 1993; Boxerman et al., 1995; Dennie et al., 1998; Kiselev and Posse, 1999). According to Eq. (3), an index of the weighted-mean vessel radius, R (often referred to as "vessel-size index (VSI)") at the baseline condition is closely related to $(\Delta R_2{}^*_{\mathrm{MION}}/\Delta R_{2\ \mathrm{MION}})^{3/2}$ (see also Eq. (14) in Tropres et al., 2001). The map of Fig. 6A shows $(\Delta R_2{}^*_{\mathrm{MION}}/\Delta R_{2\ \mathrm{MION}})^{3/2}$ (i.e., *relative* VSI) at the baseline condition, which was calculated on a pixel-by-pixel basis from the data of Figs. 1C and D. Clearly, at the surface of the cortex, high values of relative VSI were observed due to a higher ratio of large to small vessels and a longer diffusion coefficient (see the basal GE and SE CBV distribution section in Discussion). Interestingly, the white matter area (indicated by red contours) also has high values of relative VSI, which can be explained by a relatively higher ratio of large to small vessels as compared to gray matter (the diffusion constants in both gray matter and white matter are known to be similar).

A map of relative VSI for vessels undergoing dilation induced by neural activity (Fig. 6B) can similarly be determined by $((\Delta R_2{}^*_{\mathrm{stim\ +\ MION}} - \Delta R_2{}^*_{\mathrm{stim}}) / (\Delta R_{2\ \mathrm{stim\ +\ MION}} - \Delta R_{2\ \mathrm{stim}}))^{3/2}$, taking pixel-by-pixel values from the stimulation data of Figs. 2A–D. The middle of the cortex has lower relative VSI values as compared to the lower cortical area, indicating that a higher ratio of small to large vessels is contributing to the CBV change. Profiles of relative VSI across cortical layers were obtained from each animal for baseline and stimulation conditions from the two quadrangular ROIs within area 18 outlined in red in Fig. 1A. Average relative VSI values from five animals were plotted in Fig. 6C as a function of depth from the surface of the cortex. Baseline relative VSI (squares in Fig. 6C) decreases with cortical depth, with an average value of 7.23 ± 1.64 (n = 5) over the "middle of the cortex" (region shown in blue). Generally, stimulation VSI values (circles in Fig. 6C) are higher than baseline values. In the middle of the cortex, the average relative VSI value for vessels undergoing dilation during visual stimulation is 19.99 ± 7.79 (n = 5). The average ratio of stimulation to baseline values (relative VSI) in the middle of the cortex is 2.80 ± 1.08 (n = 5). If as an example the mean vessel radius was 2–5 μm in the middle cortex, then the corresponding mean vessel radius responding to stimulation would be ~6–14 μm. This is qualitatively consistent with our previous vessel diameter measurements during hypercapnic stimulation (see Fig. 8 in Lee et al., 2001). Our data strongly suggest that the dominant changes occur in vasculature with diameters larger than capillaries.

Conclusions

In our 9.4 T studies, the BOLD response is spread across cortical layers, while the CBV-weighted fMRI response is maximal at the middle of the cortex. Both CBV-weighted GE and SE fMRI have similar response functions (although the SE response is slightly sharper). The CBV-weighted GE technique has higher sensitivity and higher temporal resolution as compared to CBV-weighted SE fMRI, and therefore can be used to map sub-millimeter functional architecture (Zhao et al., 2005). Reasoning from all CBV observations across the cortex leads to the conclusions that (i) the CBV changes induced by neural stimulation are not uniform across the cortex, but are highest at the middle cortical layer,; and (ii) small arterioles and possibly venules connecting intracortical vessels and capillaries are likely to be the major source of CBV changes.

Acknowledgments

Supported by NIH (EB03375, EB03324, EB02013, NS44589, RR08079) and McKnight Foundation. We thank Drs. Hiro Fukuda, Kazuto Masamoto, Tao Jin, and Toshihiro Hayashi for insightful discussion and helpful suggestions.

References

Annet, L., Duprez, T., Grandin, C., Dooms, G., Collard, A., Cosnard, G., 2002. Apparent diffusion coefficient measurements within intracranial epidermoid cysts in six patients. Neuroradiology 44, 326–328.

Birn, R., Bandettini, P.A., 2002. The effect of T_2' changes on spin-echo EPI-derived brain activation maps. 10th Scientific Meeting of ISMRM, Honolulu. p. 1324.

Boxerman, J.L., Hamberg, L.M., Rosen, B.R., Weisskoff, R.M., 1995. MR contrast due to intravascular magnetic perturbations. Magn. Reson. Med. 34, 555–566.

Dennie, J., Mandeville, J.B., Boxerman, J.L., Packard, S., Rosen, B.R., Weisskoff, R., 1998. NMR imaging of changes in vascular morphology due to tumor angiogenesis. Magn. Reson. Med. 40, 793–799.

Duong, T.Q., Kim, D.-S., Ugurbil, K., Kim, S.-G., 2000a. Spatiotemporal dynamics of the BOLD fMRI signals: toward mapping submillimeter cortical columns using the early negative response. Magn. Reson. Med. 44, 231–242.

Duong, T.Q., Silva, A.C., Lee, S.-P., Kim, S.-G., 2000b. Functional MRI of calcium-dependent synaptic activity: cross correlation with CBF and BOLD measurements. Magn. Reson. Med. 43, 383–392.

Duong, T.Q., Kim, D.-S., Ugurbil, K., Kim, S.-G., 2001. Localized cerebral blood flow response at submillimeter columnar resolution. Proc. Natl. Acad. Sci. U. S. A. 98, 10904–10909.

Duong, T.Q., Yacoub, E., Adriany, G., Hu, X., Ugurbil, K., Kim, S.-G., 2003. Microvascular BOLD contribution at 4 and 7T in the human brain: gradient-echo and spin-echo fMRI with suppression of blood effects. Magn. Reson. Med. 49, 1019–1027.

Duvernoy, H., Delon, S., Vannson, J., 1981. Cortical blood vessels of the human brain. Brain Res. Bull. 7, 519–579.

Fujita, N., 2001. Extravascular contribution of blood oxygenation level-dependent signal changes: a numerical analysis based on a vascular network model. Mag. Reson. Med. 46, 723–734.

Harel, N., Lee, S.-P., Nagaoka, T., Kim, D.-S., Kim, S.-G., 2002a. Origin of negative blood oxygenation level-dependent fMRI signals. J. Cereb. Blood Flow Metab. 22, 908–917.

Harel, N., Zhao, F., Wang, P., Kim, S.-G., 2002b. Cortical layer specificity of BOLD and CBV fMRI signals at ultra-high resolution. Proc 10th Annual Meeting, ISMRM, Honolulu. p. 9.

Iadecola, C., Yang, G., Ebner, T.J., Chen, G., 1997. Local and propagated vascular responses evoked by focal synaptic activity in cerebellar cortex. J. Neurophysiol. 78, 651–659.

Jensen, J.H., Chandra, R., 2000. MR imaging of microvasculature. Mag. Reson. Med. 44, 224–230.

Jin, T., Tasker, M., Wang, P., Kim, S.-G., 2005. Intravascular contribution to the BOLD signal change: an echo time dependence study at 9.4 T. Proc 12th Annual Meeting, ISMRM, Miami, USA. p. 311.

Kennan, R.P., Zhong, J., Gore, J.C., 1994. Intravascular susceptibility contrast mechanisms in tissues. Magn. Reson. Med. 31, 9–21.

Kennan, R.P., Scanley, B.E., Innis, R.B., Gore, J.C., 1998. Physiological basis for BOLD MR signal changes due to neuronal stimulation: separation of blood volume and magnetic susceptibility effects. Magn. Reson. Med. 40, 840–846.

Kennedy, C., Des Rosiers, M.H., Sakurada, O., 1976. Metabolic maps of the primary visual system of the monkey by means of autoradiographic ^{14}C-deoxyglucose technique. Proc. Natl. Acad. Sci. U. S. A. 73, 4230–4234.

Kim, S.-G., Ogawa, S., 2002. Insights into new techniques for high resolution functional MRI. Curr. Opin. Neurobiol. 12, 607–615.

Kim, S.-G., Ugurbil, K., 2003. High-resolution functional magnetic resonance imaging of the animal brain. Methods 30, 28–41.

Kim, S.-G., Hu, X., Adriany, G., Ugurbil, K., 1996. Fast interleaved echo-planar imaging with navigator: high resolution anatomic and functional images at 4 Tesla. Magn. Reson. Med. 35, 895–902.

Kim, D.-S., Duong, T.Q., Kim, S.-G., 2000. High-resolution mapping of iso-orientation columns by fMRI. Nat. Neurosci. 3, 164–169.

Kiselev, V.G., Posse, S., 1999. Analytical model of susceptibility-induced MR signal dephasing: effect of diffusion in a microvascular network. Magn. Reson. Med. 41, 499–509.

Kiselev, V.G., Strecker, R., Ziyeh, S., Speck, O., Hennig, J., 2005. Vessel size imaging in humans. Magn. Reson. Med. 53, 553–563.

Lee, S.-P., Silva, A.C., Ugurbil, K., Kim, S.-G., 1999. Diffusion-weighted spin-echo fMRI at 9.4 T: microvascular/tissue contribution to BOLD signal change. Magn. Reson. Med. 42, 919–928.

Lee, S.-P., Duong, T., Yang, G., Iadecola, C., Kim, S.-G., 2001. Relative changes of cerebral arterial and venous blood volumes during increased cerebral blood flow: implications for BOLD fMRI. Magn. Reson. Med. 45, 791–800.

Lee, S.-P., Silva, A.C., Kim, S.-G., 2002. Comparison of diffusion-weighted high-resolution CBF and spin-echo BOLD fMRI at 9.4 T. Magn. Reson. Med. 47, 736–741.

Lu, H., Patel, S., Luo, F., Li, S.-J., Hillard, C.J., Ward, B., Hyde, J.S., 2004. Spatial correlations of laminar BOLD and CBV responses to rat whisker stimulation with neuronal activity localized by fos expression. Magn. Reson. Med. 52, 1060–1068.

Mandeville, J.B., Marota, J.J.A., 1999. Vascular filters of functional MRI: spatial localization using BOLD and CBV contrast. Magn. Reson. Med. 42, 591–598.

Mandeville, J.B., Marota, J.J.A., Kosofsky, B.E., Keltner, J.R., Weissleder, R., Rosen, B.R., 1998. Dynamic functional imaging of relative cerebral blood volume during rat forepaw stimulation. Magn. Reson. Med. 39, 615–624.

Mandeville, J.B., Jenkins, B.G., Kosofsky, B.E., Moskowitz, M.A., Rosen, B.R., Marota, J.J.A., 2001. Regional sensitivity and coupling of BOLD and CBV changes during stimulation of rat brain. Magn. Reson. Med. 45, 443–447.

Mandeville, J., Jenkins, B., Chen, Y., Choi, J.-K., Kim, Y., Belen, D., Liu, C., Kosofsky, B., Marota, J.J.A., 2004. Exogenous contrast agent improves sensitivity of gradient-echo functional magnetic resonance imaging at 9.4 T. Magn. Reson. Med. 52, 1272–1281.

Mchedlishvili, G., Kuridze, N., 1984. The modular organization of the pial arterial system in phylogeny. J. Cereb. Blood Flow Metab. 4, 391–396.

Ogawa, S., Lee, T.-M., Nayak, A.S., Glynn, P., 1990. Oxygenation-sensitive contrast in magnetic resonance image of rodent brain at high magnetic fields. Magn. Reson. Med. 14, 68–78.

Ogawa, S., Menon, R.S., Tank, D.W., Kim, S.-G., Merkle, H., Ellermann, J.M., Ugurbil, K., 1993. Functional brain mapping by blood oxygenation level-dependent contrast magnetic resonance imaging. Biophys. J. 64, 800–812.

Ogawa, S., Menon, R.S., Kim, S.-G., Ugurbil, K., 1998. On the characteristics of functional magnetic resonance imaging of the brain. Annu. Rev. Biophys. Biomol. Struct. 27, 447–474.

Oja, J., Gillen, J., Kauppinen, R., Kraut, M., van Zijl, P., 1999. Venous blood effects in spin-echo fMRI of human brain. Magn. Reson. Med. 42, 617–626.

Pawlik, G., Rackl, A., Bing, R.J., 1981. Quantitative capillary topography and blood flow in the cerebral cortex of cats: an in vivo microscopic study. Brain Res. 208, 35–58.

Payne, B.R., Peters, A., 2002. The concept of cat primary visual cortex. In: Payne, B.R., Peters, A. (Eds.), The Cat Primary Visual Cortex. Academic Press, pp. 1–129.

Strupp, J.P., 1996. Stimulate: a GUI based fMRI analysis software package. NeuroImage 3, S607.

Tieman, S., Mollers, S., Tieman, D., White, J., 2004. The blood supply of the cat's visual cortex and its postnatal development. Brain Res. 998, 100–112.

Tropres, I., Grimault, S., Vaeth, A., Grillon, E., Julien, C., Payen, J.F., Lamalle, L., Decorps, M., 2001. Vessel size imaging. Magn. Reson. Med. 45, 397–408.

Tropres, I., Lamalle, L., Peoch, M., Farion, R., Usson, Y., Decorps, M., Remy, C., 2004. In vivo assessment of tumoral angiogenesis. Magn. Reson. Med. 51, 533–541.

Tsao, J., 2003. Interpolation artifacts in multimodality image registration based on maximization of mutual information. IEEE Trans. Med. Imaging 22, 854–864.

van Bruggen, N., Busch, E., Palmer, J.T., Williams, S.-P., de Crespigny, A.J., 1998. High-resolution functional magnetic resonance imaging of the rat brain: mapping changes in cerebral blood volume using iron oxide contrast media. J. Cereb. Blood Flow Metab. 18, 1178–1183.

van Zijl, P.C., Eleff, S.M., Ulatowski, J.A., Oja, J.M., Ulug, A.M., Traystman, R.J., Kauppinen, R.A., 1998. Quantitative assessment of blood flow, blood volume and blood oxygenation effects in functional magnetic resonance imaging. Nat. Med. 4, 159–167.

Weisskoff, R.M., Zuo, C.S., Boxerman, J.L., Rosen, B.R., 1994. Microscopic susceptibility variation and transverse relaxation: theory and experiment. Magn. Reson. Med. 31, 601–610.

Woolsey, T.A., Rovainen, C.M., Cox, S.B., Henegar, M.H., Liang, G.E., Liu, D., Moskalenko, Y.E., Sui, J., Wei, L., 1996. Neuronal units linked to microvascular modules in cerebral cortex: response elements for imaging the brain. Cereb. Cortex 6, 647–660.

Wu, E.X., Tang, H., Jensen, J.H., 2004. High-resolution MR imaging of mouse brain microvasculature using the relaxation rate shift index Q. NMR Biomed. 17, 507–512.

Yablonskiy, D., Haacke, E., 1994. Theory of NMR signal behavior in magnetically inhomogeneous tissues: the static dephasing regime. Magn. Reson. Med. 32, 749–763.

Yacoub, E., Duong, T.Q., Van De Moortele, P., Lindquist, M., Adriany, G., Kim, S.-G., Ugurbil, K., Hu, X., 2003. Spin-echo fMRI in humans using high spatial resolutions and high magnetic fields. Magn. Reson. Med. 49, 664–665.

Zhao, F., Wang, P., Harel, N., Nagaoka, T., Kim, S.-G., 2003. Contrast agent-enhanced functional magnetic resonance imaging at 4.7T and 9.4T. Proc 11th Annual Meeting, ISMRM, Toronto. p. 1770.

Zhao, F., Wang, P., Kim, S.-G., 2004a. Cortical depth-dependent gradient-echo and spin-echo BOLD fMRI at 9.4T. Magn. Reson. Med. 51, 518–524.

Zhao, F., Wang, P., Ugurbil, K., Kim, S.-G., 2004b. Cortical Layer-dependent Basal CBV and stimulation-induced CBV Responses. Proc 12th Annual Meeting, ISMRM, Kyoto, Japan. p. 201.

Zhao, F., Wang, P., Hendrich, K., Kim, S.-G., 2005. Spatial specificity of cerebral blood volume-weighted fMRI responses at columnar resolution. NeuroImage 27, 416–424.